Annals of Nuclear Energy 142 (2020) 107387

Contents lists available at ScienceDirect

Annals of Nuclear Energy

journal homepage: www.elsevier.com/locate/anucene

Serpent/SUBCHANFLOW pin-by-pin coupled transient calculations for the SPERT-IIIE hot full power tests

Diego Ferraro [a,*], Manuel García [a], Ville Valtavirta [b], Uwe Imke [a], Riku Tuominen [b], Jaakko Leppänen [b], Victor Sanchez-Espinoza [a]

[a] Karlsruhe Institute of Technology, Institute of Neutron Physics and Reactor Technology, Hermann-von-Helmholtz-Platz 1, 76344 Eggenstein-Leopoldshafen, Germany
[b] VTT Technical Research Centre of Finland Ltd., Tietotie 3, Espoo, VTT FI-02044, Finland

ARTICLE INFO

Article history:
Received 30 September 2019
Received in revised form 27 January 2020
Accepted 11 February 2020
Available online 21 February 2020

Keywords:
Monte Carlo
Serpent 2
High-fidelity multiphysics
SUBCHANFLOW
Coupled transient calculations
SPERT-IIIE

ABSTRACT

The development of highly accurate methodologies in reactor physics requires as mandatory step a proper comparison with experimental data for relevant configurations. In this work, transient high-fidelity calculations using a recently developed coupled scheme between the Serpent 2 Monte Carlo transport code and the SUBCHANFLOW subchannnel thermalhydraulic code are done for selected reactivity insertion experiments from the SPERT-IIIE reactor. A graded approach is developed, where global and detailed results are obtained and compared with available experimental data. A good agreement is found for this novel approach, thus providing an initial step towards the validation of the tool within a configuration and operational conditions comparable to a PWR.

1. Introduction

The development of highly accurate methodologies in reactor physics, usually defined as *high-fidelity* (CASL, 2010) is oriented to provide multiphysics results through the use of calculation tools with a lower number of approximations within the modeling approach. As a general rule, the increase of such methodologies is related with the availability of extensive computational resources from High Performance Computing (HPC) infraestructures, which allow to tackle these very detailed calculations.

The European Union project McSAFE (Luigi Mercatali et al., 2017) is a coordinated effort held by 12 institutions from 7 different countries under the Horizon 2020 programme, aimed to cover this demand. Within this project, diverse coupling strategies for transient and steady-state calculations are being developed, implemented, tested and validated, mainly oriented for Pressurized Water Reactor (PWR) designs.

One of the key tools arise from the coupling between the Serpent 2 Monte Carlo (MC) code (developed by the Technical Research Center of Finland Ltd. – VTT (Leppänen et al., 2013)) and the subchannel thermalhydraulic code SUBCHANFLOW, referred here as SCF (developed by Karlsruhe Institute of Technology – KIT, Germany (Imke et al., 2012)). Diverse schemes for such approach are available (Ferraro et al., 2020; Ferraro et al., 2019; García et al., 2020), where for this work, an internal master–slave (namely embedded) coupling is considered, identified here as *Serpent-SCF*.

Previous works provided the verification of this novel approach for relevant geometries (and operational conditions) (Ferraro et al., 2020), assessing the consistency of the tool. In spite of that, the validation with experimental data for Reactivity Insertion Accidents (RIA-kind scenarios) represents a key step to assess the correctness of this proposed *high-fidelity* scheme.

For such purpose, a series of transient experiments developed in the SPERT III reactor using the E-Core (McCardell et al., 1967) (named here directly as SPERT-IIIE) are to be considered here to be calculated with *Serpent-SCF*. This 40 MW pressurized water research reactor was designed in the 1960s as part of the U. S. Atomic Energy Commission's reactor safety program, devoted to experimental and theoretical investigations of the kinetic behavior and safety of nuclear reactors.

The selected set of experiments for the SPERT-IIIE, provide RIA-kind scenarios within a PWR-type core (i.e. square lattice, oxide fuel, pin type, pressurized-water core), representing thus a first step towards validation of the proposed novel approach.

Except for its small size, this reactor has the characteristics of an unborated, commercial PWR operating with fresh fuel. The

* Corresponding author.
E-mail address: diego.ferraro@kit.edu (D. Ferraro).

https://doi.org/10.1016/j.anucene.2020.107387
0306-4549/

experiments developed were representative of cold startup, hot-startup, hot-standby and hot full power conditions of such reactors. They were initiated with a sudden withdrawal of a transient control rod, which leaded to reactivity insertions ranging from 0.5 to 1.3 $, thus providing data for non-damaging power excursions with reactor periods from 1000 to 10 ms.

Although these experiments were not developed to provide detailed pin-by-pin results, they represent the most-known experimental set of results for RIA-kind scenarios within a PWR-type core at initial conditions other than cold-startup. It should be noted that one drawback of this experimental campaign arise from the quality of available reported data, which represents a source of discrepancies, as has already been discussed by several authors (Zoia and Brun, 2016; Olson, 2013; Cao et al., 2015; Levinsky et al., 2019).

This work is then devoted to develop an initial validation of the *Serpent-SCF* for such RIA cases using the available experimental data from the SPERT-IIIE hot full power RIA tests. In addition, the main capabilities of the approach are also intended to be clearly shown in a real case scenario. In this sense, a series of sucesive steps are proposed to tackle this objectives:

1. Develop a Serpent stand-alone model to obtain Cold Zero Power (CZP) and Hot Zero Power (HZP) parameters, identifying the main relevant modeling decisions and comparing obtained results with reported experimental values.
2. Provide a rough estimation of the impact of specification uncertainties on the results.
3. Obtain and compare main core caracteristics regarding transient calculations, such as thermal feedbacks and control rod worths at Hot Full Power (HFP).
4. Select, calculate and compare global results for RIA-experiments reported, assessing the capability to reproduce the main experimental data.
5. Provide pin-by-pin results for those scenarios, in order to show potential applications of the proposed *high-fidelity* approach.

Finally, as far as the amount of CPU resources required for transient calculations based on MC is significant (Ferraro et al., 2020), a HPC is to be considered. Thus, a rough analysis of resources requirements is also provided, which represents a valuable information for the foreseen applications of the developed tools.

2. Calculation tools

The master-slave coupling approach between Serpent v.2.1.31 (as master) and SUBCHANFLOW v.3.6.1 (as slave) recently rewritten from scratch (Ferraro et al., 2020) is used in this work. This new approach incorporates all inherent capabilities from Serpent and SCF, thus allowing to develop the proposed coupled transient calculations.

2.1. Serpent 2 MC code

Serpent 2 is a multi-purpose 3D continuous-energy Monte Carlo transport code, developed since 2004 at VTT (Leppänen et al., 2013). It represents a state-of-the-art code, aimed to perform static, burnup and dynamic 3D calculations using standard ACE format Nuclear Data Libraries (NDL). It offers several geometry definition alternatives which are flexible enough to model almost all reactor geometries. In addition, the code offers inherent multi-physics features (Valtavirta, 2017), based on the combined capability to handle variable material densities fields (through methods based on rejection sampling techniques (Leppänen, 2013)) and also manage temperature fields through a rejection sampling approach combined with Target Motion Sampling (Viitanen and Leppänen, 2014). In addition these capabilities can be easily used with the definition of a mesh that superimposes such TH fields on the geometry model (namely IFCs (Serpent developer team, 2018)).

2.2. SUBCHANFLOW subchannel code

SCF is a subchannel-level thermalhydraulic code for steady-state and transient calculations developed at KIT (Imke et al., 2012), extensively used and validated for LWR. The flow solver consists of four conservation equations, namely for mass, energy, and axial and lateral momentum. The geometry is defined as a set of channels and rods with given hydraulic parameters and connectivities in a flexible manner, i. e. without assuming a particular geometry type such as square or hexagonal. In addition a geometry preprocessor allows the user to develop suitable inputs for PWR and VVER geometries through a high-level definition of lattices and geometry aspects (García et al., 2020).

2.3. Coupling approach for Serpent-SCF

The *Serpent-SCF* coupling relies heavily in the extensive use of inherent advanced features available in both codes (Leppänen et al., 2013; Valtavirta, 2017; Imke, 2018; García et al., 2020). The exchange of fields between them is handled internally using as basis the superimposed IFCs (Ferraro et al., 2020), both for the TH fields and fission power. Proper mapping files are included to consider indexing differences between each code model. In particular, for the SPERT-IIIE reactor, the control fuel assemblies are displaced axially to allow the insertion of the control rods, which has to be properly considered through according mappings.

2.4. Coupled transients with Serpent-SCF

Transient calculations are handled by Serpent as an external source case that considers both the neutrons travelling with a given position, direction and energy (identified as *live* neutrons) and another one with the precursors population that will generate the delayed neutrons (with a given decay constant per group obtained from the selected nuclear data library (Valtavirta et al., 2016)). These calculations include a time binning, where the required population control is applied (Leppänen et al., 2013). The proper generation of these sources requires a previous criticality calculation, where these sources are built. In particular, for coupled cases, these sources arise from coupled critical cases. As a result, these transient simulations with delayed neutrons in Serpent follow a two-step approach (Ferraro et al., 2020), schematically depicted in Fig. 1.

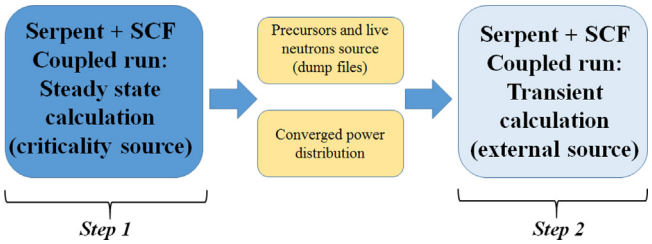

Fig. 1. Transient two-step approach for coupled calculations (Ferraro et al., 2020).

3. The SPERT-IIIE reactor

The Special Power Excursion Reactor Tests (SPERT) Project (McCardell et al., 1967) was established as part of the U. S. Atomic Energy Commission's reactor safety program in 1954. Operated by Phillips Petroleum Company, this programm consisted of a series of experiments developed in a wide range of reactor configurations, directed toward experimental and theoretical investigations of the kinetic behavior and safety of nuclear reactors. The SPERT-IIIE reactor considered in this work was a part of this program, devoted to conduct reactor behavior and safety studies under operating conditions typical of a PWR.

The reactor core configuration to be analyzed is a square lattice type, where three different rodded-type fuel assemblies (FA) can be loaded. The fuel assemblies can either be standard (SFA), control fuel type (CFA) or central (16FA), schematically depicted in Figs. 2 and 3 for the first two cases.

For reactivity control, the reactor counts with eight CFA (arranged in four pairs) and a central cross-shaped absorber, which can used to generate fast transients (namely transient rod – TR). All FA are rodded-type, formed by fresh fuel pins of low enriched uranium oxide with Stainless Steel (SS) cladding. All have the same fuel rods type and fuel pin pitch, arranged also into square lattice arrays. These FA can be either in a 5×5 pin array (SFA), an axially movable 4×4 array (CFA, where the neutron absorber box is located above the fuel pins) or in a 4×4 fixed array (16FA) that surrounds the TR.

All FAs are canned and placed into a square lattice array grid at core level. This core grid includes Zircalloy-2 guide tubes for the CFA and the central 16FA to avoid potential structural damage from the CR or TR movements. The can of the SFA includes lateral holes (with an area of 120 in^2) that could be configured to allow coolant flow between SFA, which are not present in the other FA types. Besides, for the CFA, the zone between the active fuel and the absorber include neutron flux suppressors, namely a series of plates of SS poisoned with Boron-10, which are attached to the upper fuel zone. Main aspects of these FA are presented in Table 1, where further references can be obtained directly in McCardell et al. (1967) and Olson (2015).

An scheme of the standard 60 FA reactor core configuration considered in this work is shown in Fig. 4, where the CFA and the 16FA positions are identified. As mentioned, the reactivity is controled by the movement of the central TR and the CFA, but during transients only the former is moved. In addition, the central TR includes a SS304L follower that is present in core when fully extracted. The reactor counts also with thermal shields and special SS filler boxes that fill the space between the core and the core

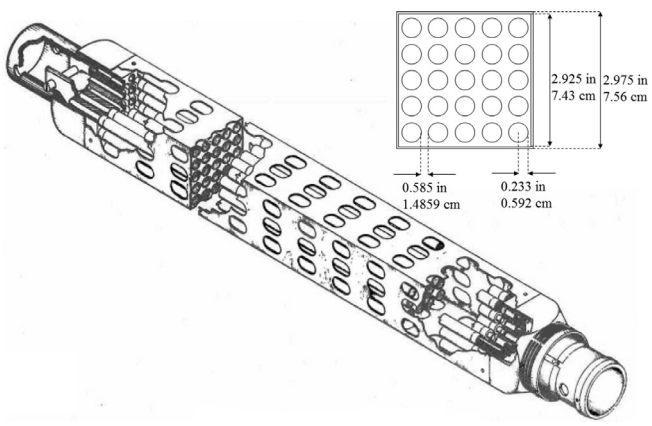

Fig. 2. Standard fuel assembly (obtained from Olson (2015)).

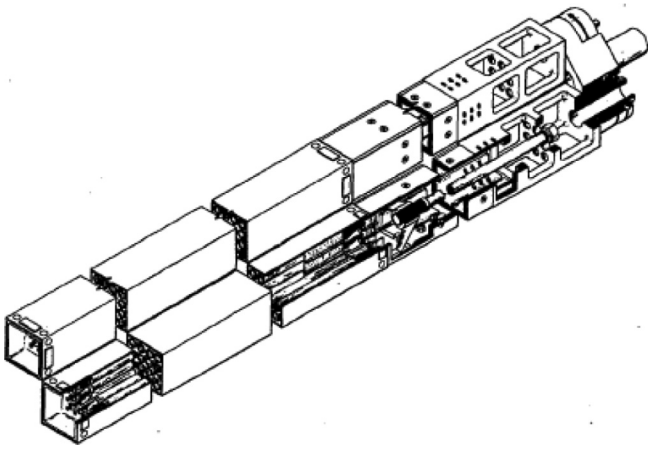

Fig. 3. Control fuel assembly (obtained from Olson (2015)).

Table 1
Main fuel data from McCardell et al. (1967).

Parameter	Value
Fuel type	Rod UO2
Clad material	SS347
Fuel density	10.5 g/cm^3
U5 Enrichment	4.8 g/cm^3
Array	Canned in SS348, 4×4 and 5×5 arrays
Fuel Rod pitch	1.4859 cm (0.585 in)
Fuel outer radius	0.5334 cm (0.21 in)
Clad outer radius	0.59182 cm (0.233 in)
Clad inner radius	0.54102 cm (0.213 in)
Clad thickness	0.0508 cm (0.02 in)
Active length	97.282 cm (38.3 in)
FA pitch	7.62 cm (3 in)
Gap between FA	0.0635 cm (0.025 in)
Nominal	998.03 kg/m3 at (294 K, 101.35 kPa)
moderator	947.4324 kg/m3 at (394 K, 10.34 MPa)
density	790.9624 kg/m3 at (533 K, 10.34 MPa)
Nominal	294 K (Cold)
inlet	394 K (Hot Standby-1)
temperature	533 K (Hot Standby-2)

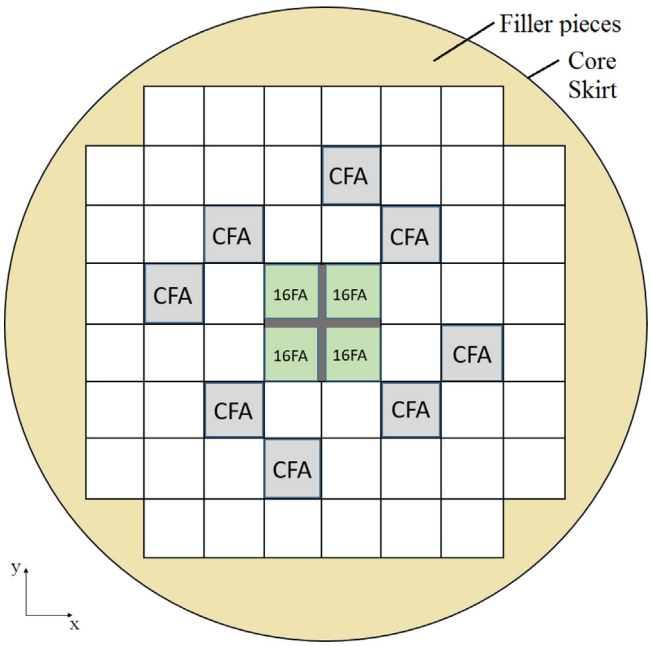

Fig. 4. Core scheme. Central TR in grey. White positions identify SFA.

Table 2
Main core data from McCardell et al. (1967) and Olson (2015).

Parameter		Value	
		Fuel assembly	
Type	Number	External can size	Flow area
25 rod assembly	52	7.56 cm (2.975 in) × 7.56 cm (2.975 in) × 133.99 cm (52.750 in)	27.68 cm^2 (4.29 in^2)
16 rod assembly	4	6.29 cm (2.476 in) × 6.29 cm (2.476 in) × 133.99 cm (52.750 in)	20.39 cm^2 (3.16 in^2)
CFA	8	6.34 cm (2.496 in) × 6.34 cm (2.496 in) × 115.93 cm (45.64 in)	18.06 cm^2 (2.8 in^2)
		Core details	
Nominal power		40 MW max	
Inlet pressure		14.7 to 1500 psia (1.0135 to 10.34 MPa)	
Control system		1 transient rod (cruciform)	
Absorber		4 control assemblies in pairs (square tubes)	
Material		1.35% B10 in SS304L 3/16 in (0.47625 cm) thick for TR, 0.186 in (0.47244 cm) for CR	
Shield materials		SS304L	
		Support grids	
Position		Material	Thickness
Upper		304L SS	17.78 cm (7 in)
Lower		304L SS	7.62 cm (3 in)

skirt, which act as neutron reflectors. Main global characteristics of the core and FA arrays are listed in Table 2.

3.1. Hot full power excursion tests: analyzed RIA-type scenarios

The proposed scenarios to be analyzed in this work are obtained from reported experimental tests (McCardell et al., 1967). The selected cases depart from a critical converged hot full-power state at 20 MW, to proceed to a fast reactivity insertion due to the TR withdrawal. These scenarios are named as T-84 and T-85, where it should be regarded that no initial CR position is reported. Main aspects are summarized in Table 3, where the reported experimental uncertainty is included. The sources of this uncertainty can be gathered directly in McCardell et al. (1967), together with the main description of the experimental measurement details.

4. Models developed

4.1. Serpent neutronics model

Several relevant modeling decisions are mandatory as far as the main specification available lacks from details on diverse key core components. Available open publications show a big discrepancy on several of these aspects (Zoia and Brun, 2016; Olson, 2013; Cao et al., 2015; Levinsky et al., 2019), where differences in core compositions (namely impurities of structural materials), guide tubes sizes and can thickness are easily identifiable. Those differences have an important impact on main core parameters, as it will be presented in the following sections. Besides, the available experimental results for stationary core parameters (such as core reactivity, control rod worth, etc) also show a big discrepancy between diverse reported experimental measurements (Zoia and Brun, 2016).

As a consequence, to develop the transient scenarios proposed, a Serpent model was developed based in traceable decisions, which more relevant are:

a. All core relevant components such as SFA, CFA, TR, reflectors, etc. were modeled following the available dimensions in McCardell et al. (1967).
b. As recommended in Olson (2015), SS348 was considered instead of SS347 for fuel cladding.
c. A mass of 50 g of SS348 was considered for the intermediate spacer grids of the SFA, positioned according to McCardell et al. (1967). A scaled mass was used for the CFA and central fuel assemblies.
d. The main material compositions were obtained directly from RJ McConn (2011), except for the fuel, where compositions from Olson (2015) are considered.
e. The gap between outer Zircalloy 2 guide tubes and FA preserve the same gap as for the FAs.
f. The thickness of Zircalloy-2 guide tubes for the central FA was obtained considering 0.025 in (0.0635 cm) gap between outer FA can and the guide tube and 0.125 in (0.3175 cm) between the guide and the CR. This resulted in ∼0.3 cm thickness of Zircalloy for the central FA.
g. The thickness for the control fuel assemblies Zircalloy 2 guide tubes was obtained considering 0.075 in (0.1905 cm) gap between the CFA fuel zone and the guide tube, resulting in a thickness of ∼0.4175 cm (0.1645 in).
h. The thickness of the SS can for all fuel assemblies was obtained considering the outer size and the flow area, resulting in 0.0639 cm, 0.0626 cm and 0.1837 cm thickness for the 5 × 5 fuel assembly (SFA), the 4 × 4 (16FA) and the CFA respectively.
i. The lateral can holes of the normal (5 × 5) fuel assembly were homogenized, resulting in ∼75% SS and ∼25% of coolant in volume.
j. The zone between the active fuel and the hollow absorber of the CFA was homogenized considering the volume of pins, cans and flux suppressors.
k. A constant gap conductance is considered (of 10 e3 $W/m^2/K$) for the transients (typical value for PWR).
l. Independent coolant materials for the core inlet and outlet were considered.

Table 3
Selected experiments to be analyzed.

ID	Reactivity insertion [$]	Inlet temp. [K]	Flow rate [gpm]/[lps]	Initial Power [MW]	Max. Power [MW]	Time to peak power [s]
T-84	0.46 ± 0.02	536.15 ± 2	12000/ 757.1	19 ± 1	39 ± 4	0.18 ± 0.02
T-85	0.87 ± 0.04	535.15 ± 2	12000/ 757.1	19 ± 1	130 ± 10	0.155 ± 0.005

m. The coolant and fuel temperatures and densities in the inner fuel assemblies were modified using proper nested IFC meshes, considering a pin-by-pin coupling with 20 axial zones.
n. JEFF3.1.1 (Santamarina et al., 2009) ACE NDL distributed with Serpent was used, where it should be noted that the delayed neutron data is condensed to 8 precursors groups.

The main aspects of this model can be observed in the plots presented in Figs. 5–8. Besides, superimposed mesh power detectors (Serpent developer team, 2018) were included in the model to obtain the power generated by fission, modelling the whole energy release as deposited in the respective bin. As a result, further sections will present pin-by-pin results using these square lattice detectors by FA, which include an axial discretization of ~5 cm.

4.2. SUBCHANFLOW TH model

The same approach was followed for the SCF model, which was developed considering the following aspects:

- A coolant-centered model was selected, as shown in Fig. 9.
- The same axial discretization as for the Serpent model IFC was considered (i.e. 20 axial zones, selected according to previous experience).

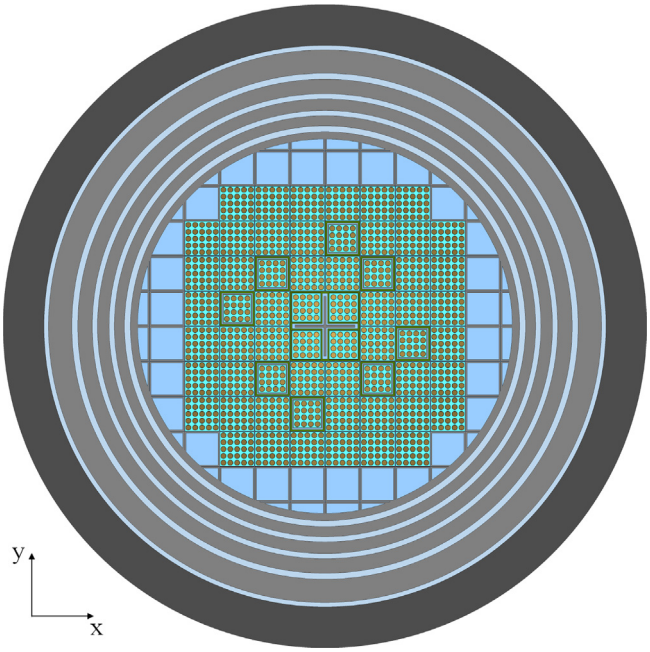

Fig. 5. Serpent model x-y cut at centre of core. Plot for HFP (higher opacity represents lower temperature).

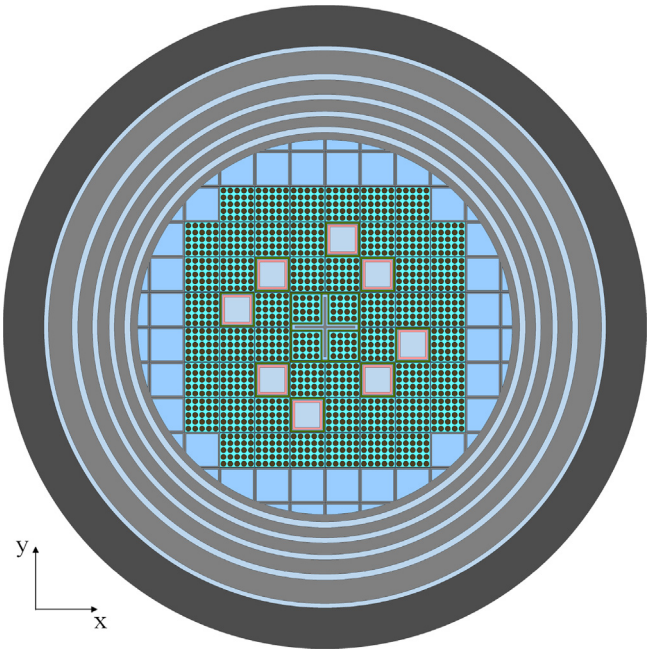

Fig. 7. Serpent model x-y cut at centre of core. CR inserted.

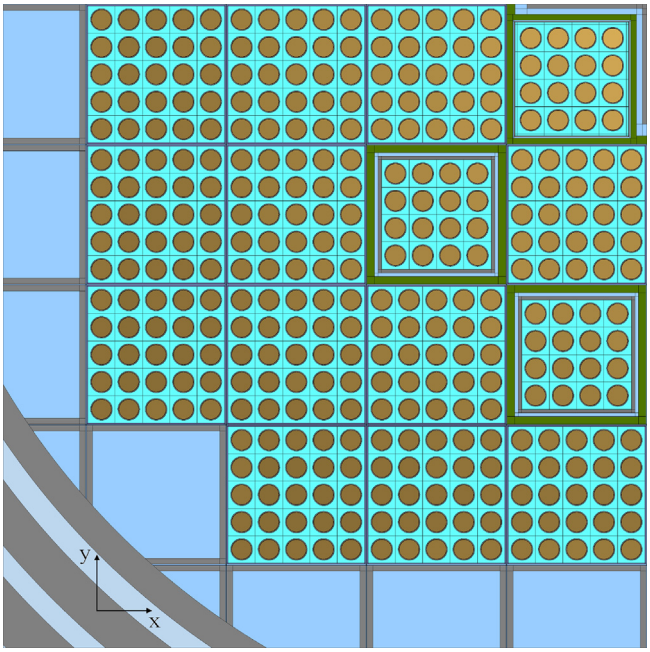

Fig. 6. Serpent model x-y cut at centre of core. Detail of CR and TR.

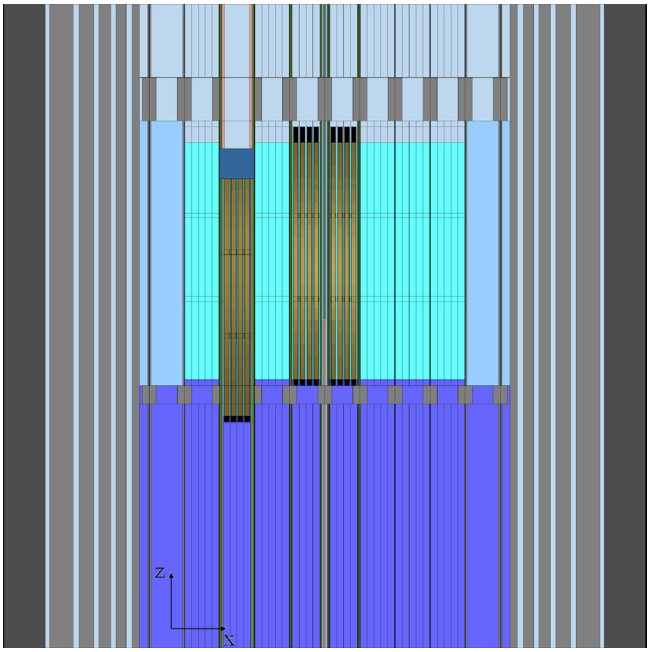

Fig. 8. Serpent model x-z cut 6 cm from centre of core. CR inserted 25 cm.

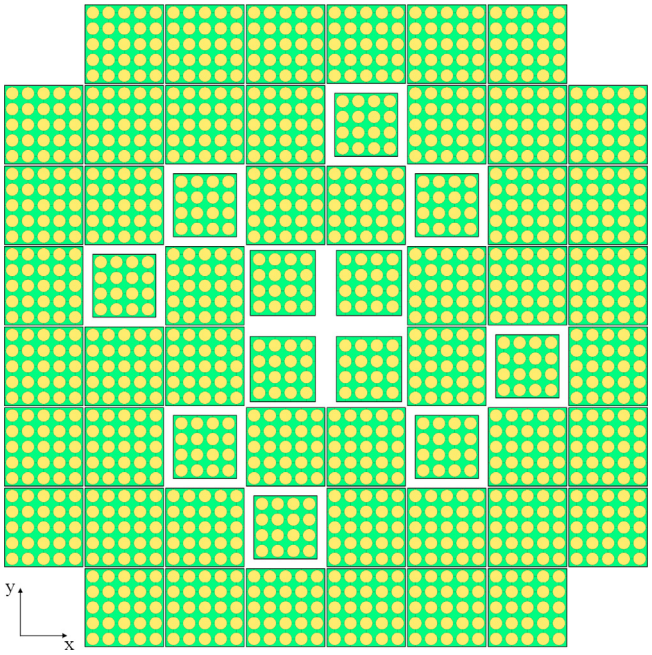

Fig. 9. SCF model – plot obtained from preprocessor García et al. (2020).

- No cross-flow between FA was considered (i.e. it was considered that SFA were arranged in such way).
- The main input was constructed through a preprocessor that generates the geometry files to define channels and rods, as well as connections between them. The mapping files were also obtained from this preprocessor.
- The convergence criteria for the TH solution was selected to be at least one order of magnitude below the coupling convergence criteria for the steady-state calculation.

4.3. Coupling options and running environment

Volume averaged fuel temperatures were considered for the TH feedback. For steady-state calculations at HFP, a proper convergence in L_2 norm was set (Ferraro et al., 2020). In addition, for the transient calculations a fully-explicit scheme was considered for the time integration of the coupling scheme. Due to the high level of computational resources required for these calculations, a HPC was considered up to 50 nodes of 20 CPUs each (i.e. 1000 Intel(R) Xeon(R) CPU E5-2660 v3 @ 2.60 GHz in total). For such purpose a compilation of the coupled tool with the Hybrid MPI-OMP implementation of Serpent was considered, while the SCF part was run sequentially.

5. Results

A series of global and detailed analysis are to be presented and briefly discussed in a graded approach in this section. These analysis are aimed both to provide a preliminary validation and verification of the implementation and also to show main *high-fidelity* capabilities now available. For completness, these results are presented including the associated statistical uncertainty (identified as *Stdev*), indicating the number of σ considered.

As a first step, stand-alone Serpent runs are done to assess the main model aspects, verifying the consistency of the main modeling decisions (items a to n on Section 4.1). Afterwards, diverse coupled *Serpent-SCF* calculations are performed, firstly as steady state (to obtain the *live* neutron and precursors source) and finally as coupled transient cases (to obtain results for cases T-84 and T-85). The main description of runs types is presented Table 4.

Table 4
Main coupled S-SCF cases specifications.

#	Type of run	Used for	Main run parameters
I	Criticality run (coupled and uncoupled)	Main results / Obtain precursors and live neutron files	3e8 / 9e8 active histories (3000 cycles)
II	External source with delayed neutrons (coupled)	Main results for T-84 and T-85 cases	2e6 active histories per time bin

It has to be regarded that the comparison with experimental results is expected to provide a level of agreement in the order of ∼1–1.5 β for core reactivities (such as TR reactivity worth, excess reactivities, etc.), in accordance with the specification quality (as reported in similar works, such as (Zoia and Brun, 2016; Olson, 2013; Cao et al., 2015; Levinsky et al., 2019)). In this sense, some discrepancies arising from the specifications in McCardell et al. (1967) and Olson (2015) are expected, which will be tackled with a rough sensitivity analysis.

Moreover, in view of the foreseen transient cases proposed in Table 3, it is important that the main parameters governing the time evolution of the coupled case are correctly modeled (such as kinetic parameters and isothermal reactivities), where differences below ∼5% are expected. Finally, for the transient calculations, the proper modeling of the whole time evolution is expected within both experimental and calculation uncertainties, where the correct modeling of power peak is considered as a key factor. In this point it should be regarded that for these HFP transients the experimental uncertainties (McCardell et al., 1967; Olson, 2015) are reported only for the initial time and the peak power, where the values are ∼5% and ∼10% respectively (as shown in Table 3). As a consequence, it will be considered a good agreement the correct representation of the power peak within the reported experimental uncertainty, together with the full time scope agreement with diferences between ∼5% to ∼10%.

5.1. Serpent 2 stand-alone model

The reported values present a wide spread in diverse SPERT-IIIE reports, thus a decision to verify the most relevant parameters was done. In this sense, a level of agreement with reported data as for that already reported by several authors (Zoia and Brun, 2016; Olson, 2013; Cao et al., 2015; Levinsky et al., 2019) is expected. For such reason, the following experimental values were here assessed, all of them obtained with uncoupled Serpent runs:

i. Main core reactivities for CZP.
ii. Impact of specification uncertainties in CZP reactivity.
iii. Isothermal reactivities.
iv. Transient rod reactivity worth at CZP and HZP.

5.1.1. Main core reactivity parameters at CZP

The main results for static reactivities at CZP are presented in Table 5, where the cases with all rods out (ARO) and with transient rod in (and CR out) are presented. In addition a configuration reported as critical in other publications (Levinsky et al., 2019; Zoia and Brun, 2016), identified as *Case A*, is also calculated.

The comparison with reported experimental values is presented in Table 6. It can be observed that a good agreement is encountered for all parameters, although a reactivity offset is found, which will be analyzed in the following section. This effect has already been pointed out in other works (Cao et al., 2015; Olson, 2013), where

Table 5
Serpent results for the CZP (Uncoupled). *Stdev* for Serpent at 1σ.

Case	k_{eff}	β^1_{eff} [pcm]	Rho [pcm]	Rho [$]
ARO	1.0962 ± 6E−5	748.8 ± 3.0	8775 ± 5	11.7 ± 6E−3
TR in	1.0594 ± 6E−5	762.0 ± 3.2	5603 ± 5	7.4 ± 7E−3
CaseA[2]	0.9695 ± 7E−5	768.6 ± 3.5	−3142 ± 7	−4.1 ± 9E−3

[1]Calculated with IFP (iterated fission probability method) (Serpent developer team, 2018).
[2]CR 72.644 cm, TR out.

Table 6
CZP results comparison with reported values from Olson (2015). *Stdev* for Serpent at 1σ.

Parameter	Measured	Calculated	Difference
Excess ρ [$]	13.1 ± 0.7	11.7 ± 6E−3	1.4
TR Worth [$]	4.6	4.4	0.2
$\beta_{eff}/\Lambda_{eff}$ [ms]	2.15 ± 0.008	2.03±0.01[1]	0.12
CaseA[2] ρ [pcm]	0	−3142 ± 7	−3142

[1]Calculated with IFP (iterated fission probability method) (Serpent developer team, 2018).
[2]CR 72.644 cm, TR out.

Table 7
Impact of uncertainty specifications in reactivity results for CZP.

#	Case description	ρ [pcm]	ρ [$]
a	No intermediate grids	315	0.41
b	No flux suppressors (ARO)	30	0.06
c	1 mm less Zr in central guide tubes	40	0.09
d	1 mm less Zr in CFA	400	0.64
e	No Tantalium in SS348	690	0.81
f	CZP ARO with ENDF/B VII.0	-76	−0.1

on each case a modeling decision to compensate such offset was held. In addition, the CR from CFA shows an increased reactivity worth with respect to reported values.

5.1.2. Impact of specification uncertainties on main results

As previously mentioned, the main documentation shows a lack of specification on key core parameters that are expected to impact in the excess reactivity. The main modeling decision was to avoid the adjustment of such parameters, but to provide a proper quantification of the impact of each of these decisions. For such purpose, a rough analysis of the effect of main specification uncertainties was held, considering the following cases:

a. The impact of the consideration of intermediate grids in FA.
b. The consideration of flux suppressors for CFA.
c. The impact of the central fuel Zircalloy guide tubes.
d. The impact of the CFA Zircalloy guide tubes.
e. The impact of impurities on SS348 (f.e. the concentration of Tantalium).

These items arise from the analysis of reactor data from McCardell et al. (1967) and Olson (2015), where the most easily identifiable are here considered. The results obtained for such cases are presented in Table 7. For completness, an additional calculation of the same CZP ARO case using ENDF/B VII.0 NDL (Chadwick et al., 2011) is also included, identified as case *f*. This latter case is given in order to provide a rough estimation of the impact of nuclear data on the static reactivity results.

From a rough analysis of results of Table 7, it could be easily expected a reactivity offset of ±1.5$ from the main specification uncertainty, where further differences could be also expected from other components specification and from the data within the NDL.

5.1.3. Isothermal reactivities calculation

The main results for the isothermal reactivity are obtained and compared with reported ones (obtained from (Levinsky et al. (2019)), as shown in Fig. 10. It can be seen that a good agreement is observed, with differences between 0.8 to 1.3 β_{eff}.

5.1.4. Transient Rod reactivity worth for CZP and HZP

The main results for the transient rod reactivity worth are obtained and compared with reported ones both for CZP and HZP cases (obtained from McCardell et al. (1967), as shown in Fig. 11). For both cases an initial CFA position near critical was considered. It can be seen that a very good agreement is observed, with differences between 0.1 to 0.5 β_{eff}.

5.1.5. Summary of main aspects from Serpent stand-alone model

The results shown in previous sections assess the accuracy level for this SPERT-IIIE model at steady-state and its main kinetic

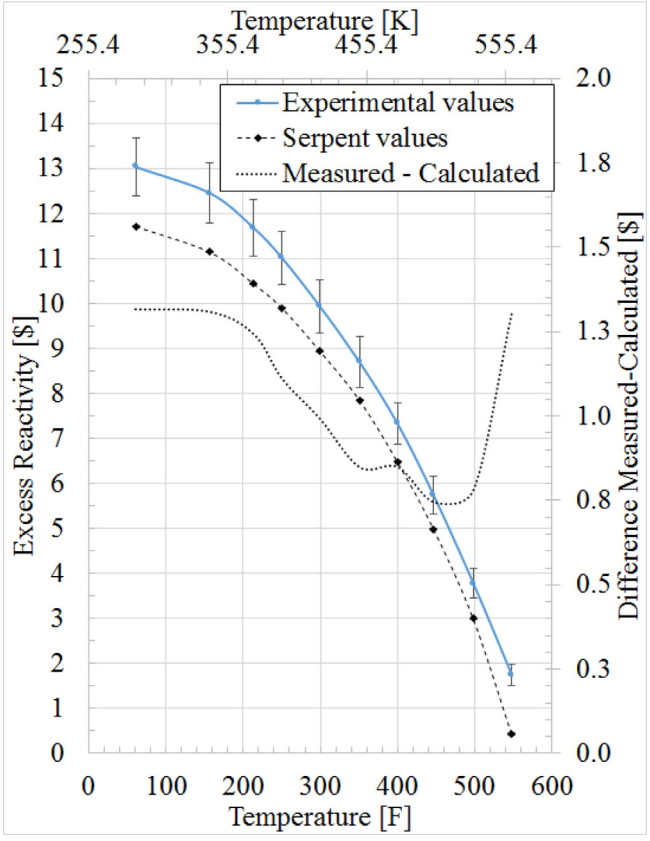

Fig. 10. Measured and calculated excess reactivity versus isothermal temperature – *Stdev* for *Serpent-SCF* at 2σ.

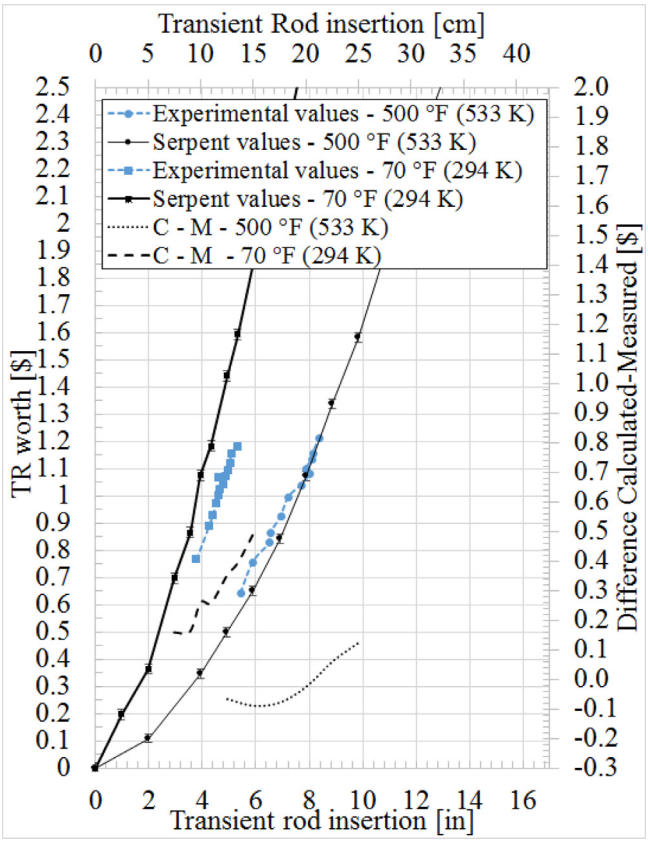

Fig. 11. Measured and calculated TR reactivity worth – *Stdev* for *Serpent-SCF* at 2σ.

parameters that will affect the further transient calculations. In this sense it should be regarded that:

- Despite the difference in the CFA reactivity worth, the actual starting positions during the transients are not reported. As far as those values are to be nevertheless adjusted, no impact on the further calculations are expected.
- The reactivity offset observed due to lack of specification has the same impact as the last item.
- The main core parameters that define the transient behaviour (i.e. TR reactivity shape, isothermal reactivity change and core kinetic parameters) are modelled with very good agreement with reported experimental values. As a consequence, a good capability to represent the proposed transient tests should be expected if the proposed implementation is consistent.

5.1.6. Serpent-SCF steady-state critical case hot at full power

A critical (coupled) configuration at 20 MW was obtained through successive iteration. For such cases, the TR was adjusted to be able to introduce a maximum reactivity of ~1 β_{eff}. As a result, the CR position was found to be ~15 cm of extraction and ~25 cm of insertion of TR. The convergence criteria was set to 20 K and 2.5 K for fuel and coolant temperatures respectively and to 0.01 for the variation in density, using a 0.5 relaxation of TH fields between iterations. The converged power densities are presented in Figs. 12–14 for axial and lateral cuts, while the obtained temperatures are presented in Figs. 15 and 16. As previously mentioned, this case was used to get the steady-state source of precursors and *live* neutrons to be used for further transient calculations.

Finally, in order to get the reactivity to be introduced by the TR withdrawal, several additional criticality calculations were developed for diverse TR withdrawals. The results are presented in Fig. 17.

5.2. Serpent-SCF coupled transient cases

For both cases listed in Table 3, a transient calculation of 1 s lenght with 100 bins were considered (i.e. 10 ms per time bin). For each case, a TR withdrawal that inserts the corresponding reactivity peak reported in Table 3 is considered. The TR withdrawal scenario considered is summarized in Table 8 for each case, where a constant speed is modeled for simplicity, after which the movement stops. It should be noted here that slight differences are foreseen, as far as no specification of this TR movement is reported in McCardell et al. (1967).

To take into account the global experimental uncertainties for both cases, the reported experimental errors are included in the power and reactivity experimental results plots. For the reactivity, a 4% is considered (as proposed in (Olson, 2015)), while the power plots are presented including the initial reported uncertainty (~5%), where it should be regarded that the uncertainty near the power peak is reported to be ~10% for both cases.

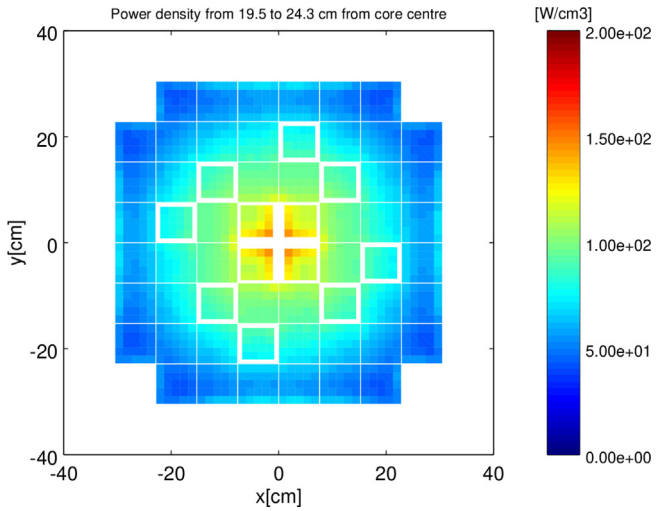

Fig. 12. Power density x-y cut 20 cm above core centre – critical converged configuration at 20 MW.

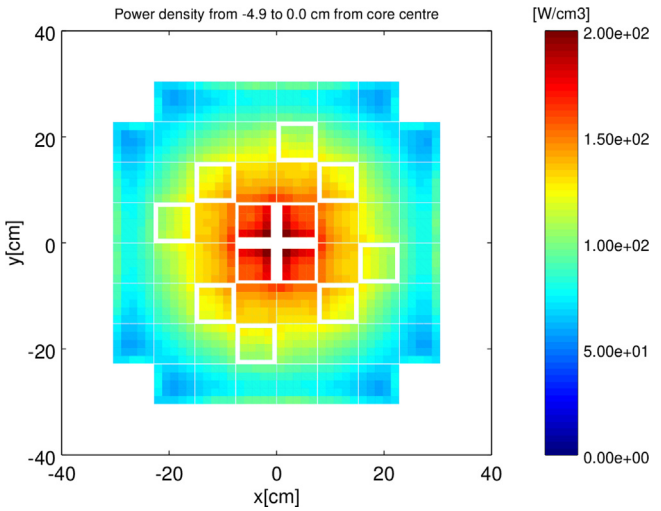

Fig. 13. Power density x-y cut at core centre – critical converged configuration at 20 MW.

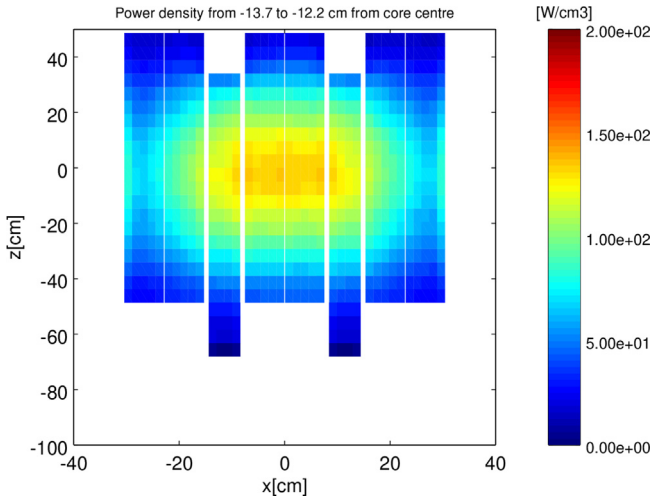

Fig. 14. Power density at x-z cut at CFA – critical converged configuration at 20 MW.

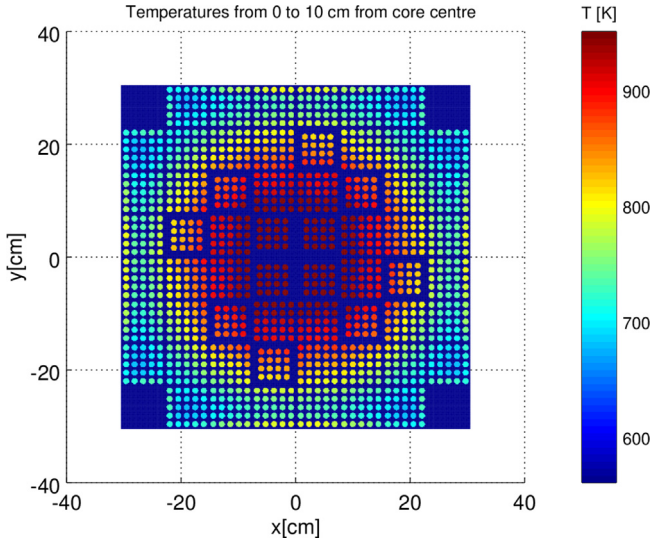

Fig. 15. Temperatures at x-y cut at core centre – critical converged configuration at 20 MW.

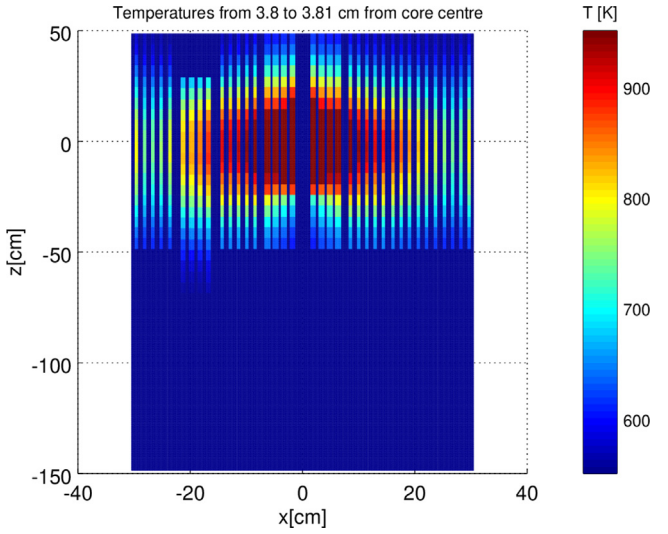

Fig. 16. Temperatures at x-z cut at CFA – critical converged configuration at 20 MW.

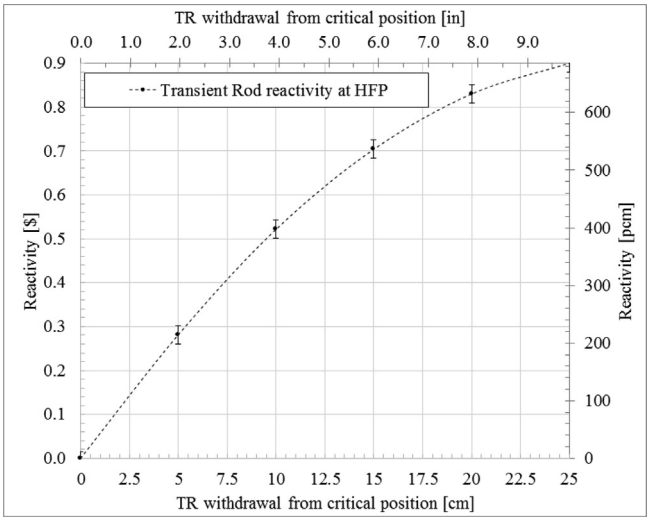

Fig. 17. Reactivity insertion for transient rod reactivity withdrawal from critical position at 20 MW – *Stdev* for *Serpent-SCF* at 2σ.

Table 8
Modeled TR withdrawal scenarios.

Case	TR movement [cm]	Speed [cm/s]	Time scope [s]	bins
T-84	8.7	−67.1	0.04–0.17	100
T-85	22.9	−190.8	0.04–0.16	100

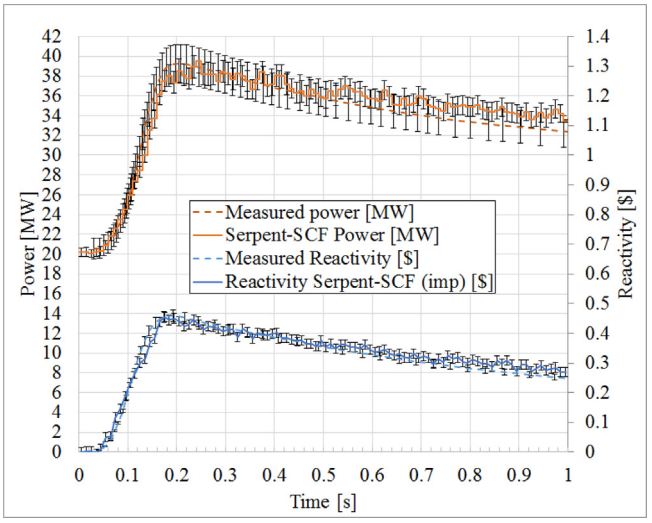

Fig. 18. Main results for Test 84 – *Stdev* for *Serpent-SCF* at 2σ.

5.2.1. Results for T-84

Given the specifications of Test 84 in from Table 4, an according TR extraction was modelled. Fig. 18 presents the global results obtained comparison with reported experimental ones, where the total power is presented together with an estimated inserted reactivity (obtained from the implicit estimator).

It can be observed from Fig. 18 that a good behavior is observed and all the aspects of the transient are modeled correctly by *Serpent-SCF*, where the increase of average temperature provides the negative feedback to balance the inserted reactivity by the RIA. The global evolution is found to be within the experimental

uncertainty for both reactivity and power results. A slight difference in the reactivity is observed near the power peak, which is reflected as a slight offset of the power evolution near this time. This slight difference is indicating that a more detailed TR movement should be used to obtain an exact match. In spite of that, no further adjustment of the CR movement was held as far as the main purpose here is to correctly model the global evolution and the consistency of the feedbacks.

Being the global behaviour consistency checked, the *high-fidelity* capabilities can be analyzed. As an example, the power increase at pin-level are shown in Figs. 19 and 20, obtained from the pin power detectors. For such pin-by-pin results, the average *Stdev* in power is ~1–1.5% and the maximum is below 9% (located in the bottom of CFA, below 3% for the rest of core).

Regarding the temperature evolution, Figs. 21 and 22 present an axial cut for the differences with respect to initial time at 0.2 and 0.5 s respectively.

5.2.2. Results for T-85

The Test 85 from Table 4 represents a higher reactivity insertion, thus higher power peak and temperature increases are expected. The Fig. 23 presents the comparison of global results with experimental ones for this case, where again the total power is presented together with an estimated reactivity (obtained from the implicit estimator).

It can be observed from Fig. 23 that a good behavior is observed and again all the aspects of the transient are modeled correctly by *Serpent-SCF*. The higher power peak is correctly represented and the TH feedbacks are consistent. As for the case T-84, a slight difference in the reactivity introduced is observed, also indicating that a more complex TR movement should be used to obtain an exact match. Again no further adjustment of the CR movement was held as far as the main purpose here is to correctly model the global evolution and the consistency of the feedbacks.

As for the T-84 case, being the global behaviour consistency checked, the *high-fidelity* capabilities can be analyzed. The power increase at pin-power are shown in Figs. 24 and 25, obtained from the same pin power detectors as for the case T-84. For such pin-by-pin results, the average *Stdev* in power is ~1–1.5% and the maximum is below 9% (located in the bottom of CFA, below 3% for the rest of core).

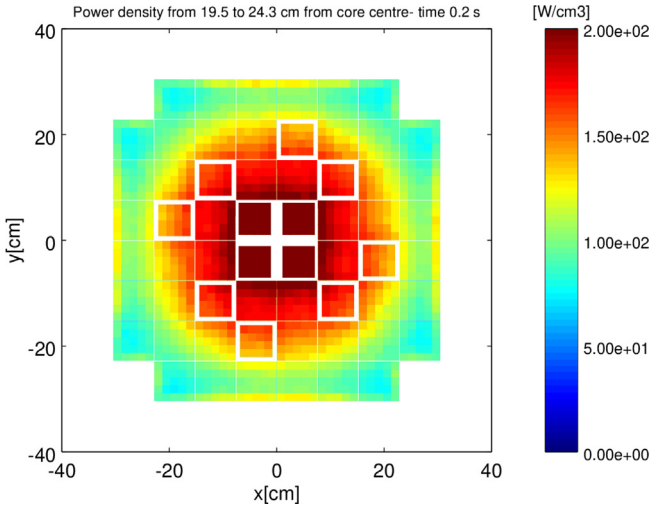

Fig. 19. Pin power results for Test 84 – x-y cut, time 0.2 s.

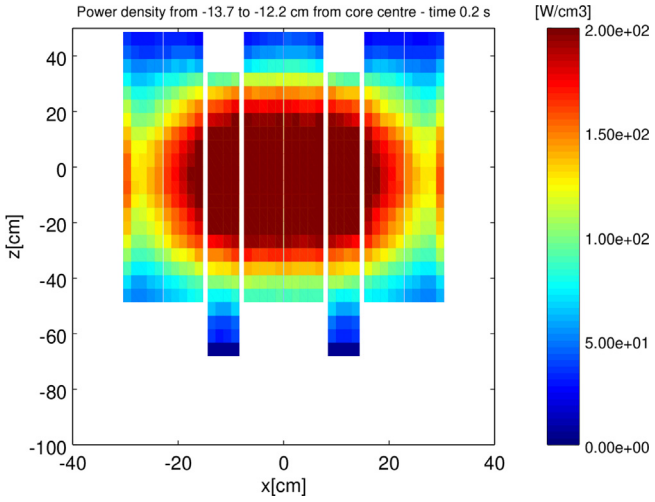

Fig. 20. Pin power results for Test 84 – x-z cut, time 0.2 s.

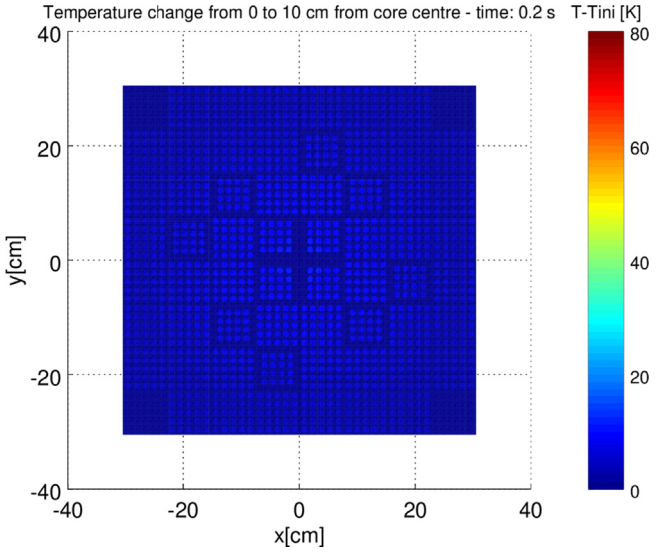

Fig. 21. Difference in temperature – results for Test 84 – x-y cut, 0.2 s vs initial time.

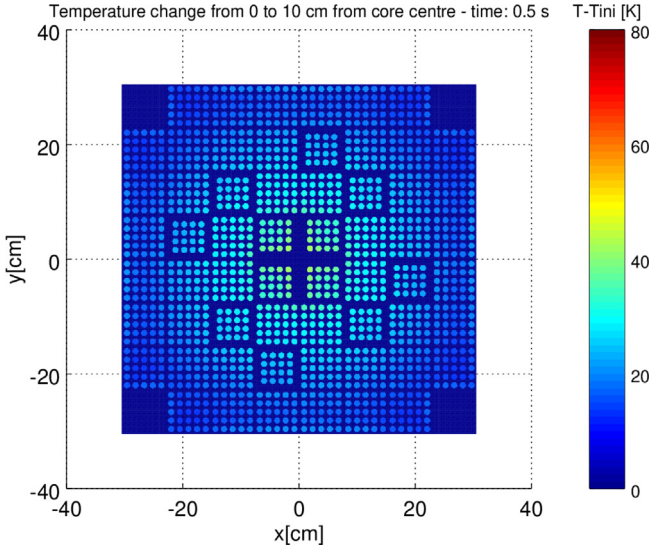

Fig. 22. Difference in Temperature – results for Test 84 – x-y cut, 0.5 s vs initial time.

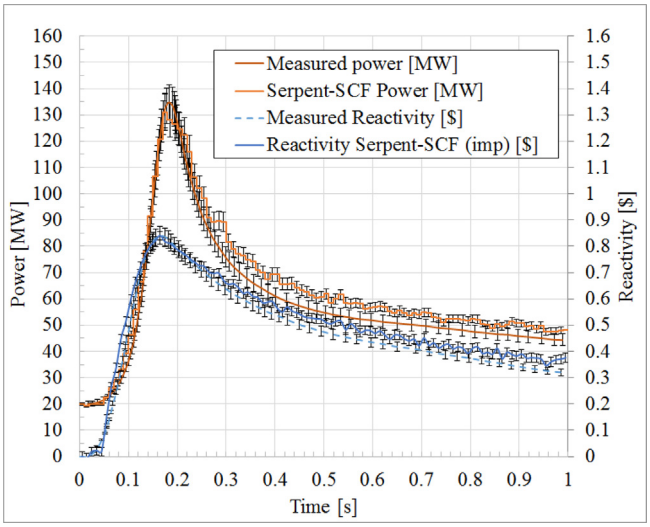

Fig. 23. Main results for Test 85 – *Stdev* for *Serpent-SCF* at 2σ.

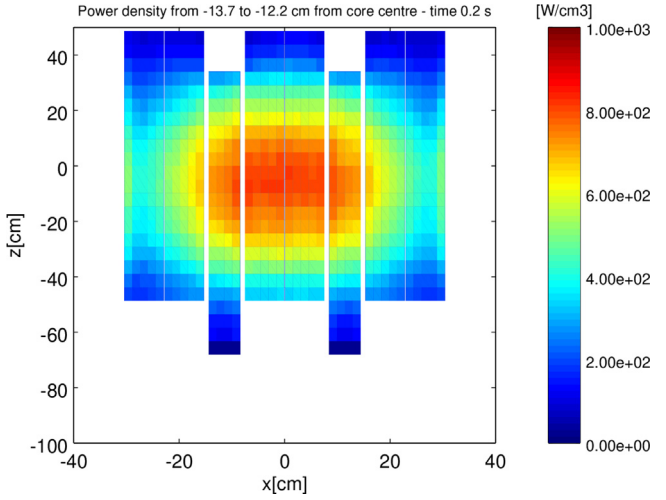

Fig. 25. Pin power results for Test 85 – x-z cut, time 0.2 s – limits of color bar increased respect to Fig. 13.

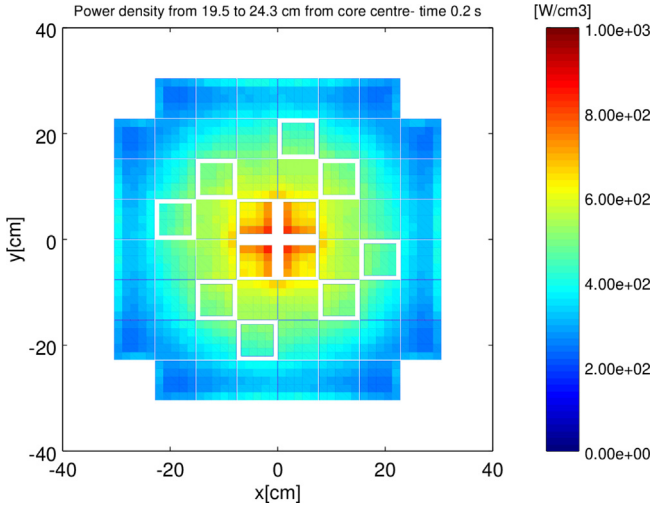

Fig. 24. Pin power results for Test 85 – x-y cut, time 0.2 s – limits of color bar increased respect to Fig. 12.

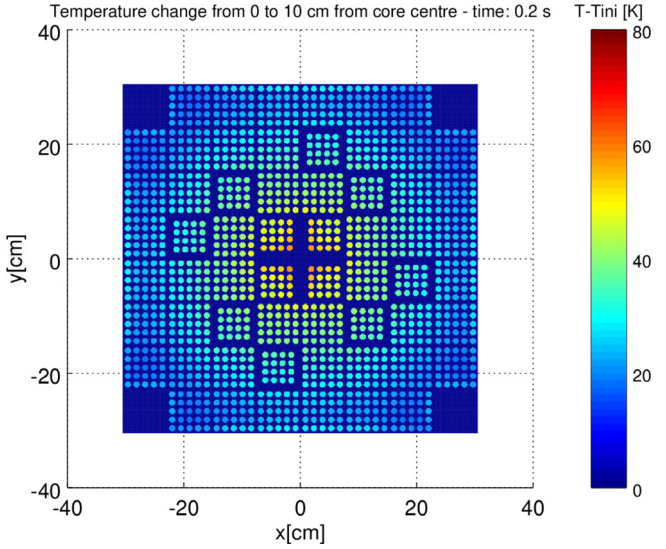

Fig. 26. Difference in Temperature - results for Test 85 – x-y cut, 0.2 s vs initial time.

For the temperatures evolution in this case, Figs. 26 and 27 present the same axial cut showing the changes with respect to initial time at 0.2 and 0.5 s, where it can be easily observed that the increase is clearly higher as for the T-84 case.

It has to be regarded that the main feedback for these cases arise from fuel temperatures, as far as the time scope is short. In order to show this effect, the Fig. 28 shows the same power evolution comparison as for Fig. 23, together with the evolution of coolant and fuel temperatures, where it can be seen that the increase on the former are only ~2 K.

5.2.3. Comparison of maximum power

Finally, the comparison of experimental and calculated results for the maximum power for cases T-84 and T-85 from Figs. 18 and 23 is presented in Table 9, where it can be seen that the differences encountered are within the reported experimental uncertainty.

5.2.4. Involved computational resources

As previously mentioned, one of the main constrains of these MC coupled calculations is the amount of computational resources involved, already seen in previous verification works (Ferraro et al., 2020). A brief summary of resources for these transient problem is presented in Table 10 for a given time bin of the calculation. It is worth to note here that the initial steady-state calculation to build the initial source is not considered.

It can be seen from Table 10 that the CPU resources required for these transient coupled MC calculation are significant and can potentially represent a limiting factor. With the aim of the HPC used in this work, each complete transient scenario could be run in about ~5–10 h using 1000 processors in total to model the complete the 1 s scope. This fact should be considered if no vast computational resources are available. Fortunately, the scalability of Serpent in similar architectures has already been analyzed for similar problems (Ferraro et al., 2018), showing that the real time for the Serpent run can be still reduced just adding additional nodes. On the contrary, other parts of the problem (such as the field mapping and the SCF calculations) are not inherently parallel as MC transport calculations, which sets an upper boundary to this scalability.

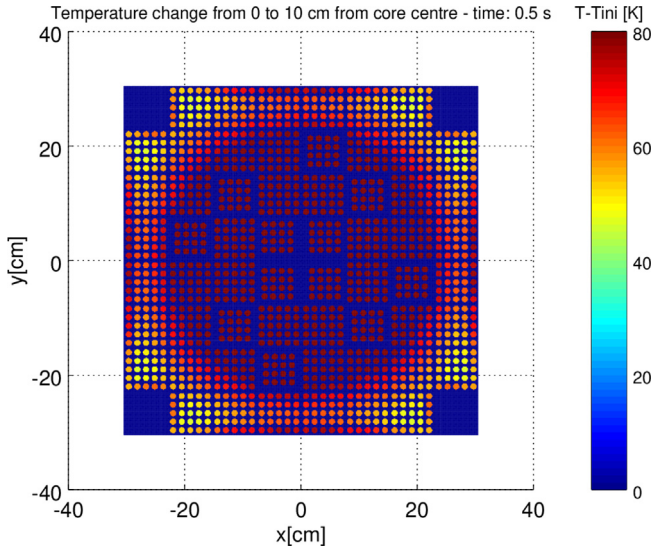

Fig. 27. Difference in Temperature – results for Test 85 – x-y cut, 0.5 s vs initial time.

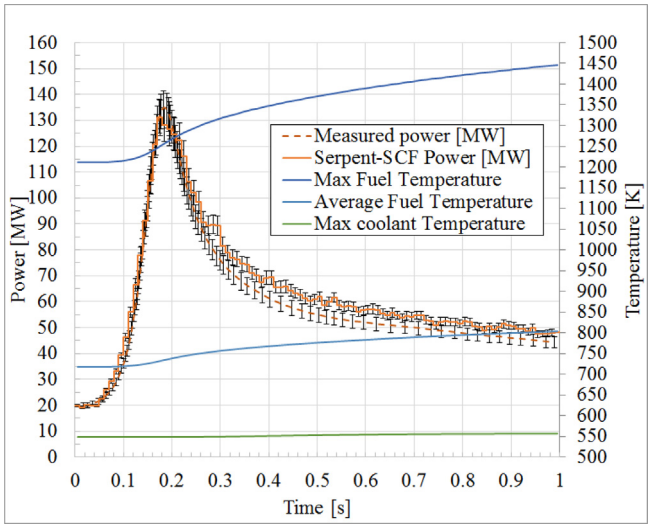

Fig. 28. Main power and Temperature results for Test 85 – *Stdev* for *Serpent-SCF* at 2σ.

Table 9
Power peak comparison with experimental values – *Stdev* for *Serpent-SCF* at 2σ.

Case	Reported (McCardell et al., 1967; Olson, 2015) [MW]	Calculated [MW]
T-84	39 ± 4	39.6 ± 1.2
T-85	130 ± 10	131.1 ± 6.8

Table 10
Associated running times of the coupling scheme.

Code	CPU time per time bin [mins][1]
SCF run	$\sim 4.0E-01$
Serpent run	$\sim 4.0E+03$

[1] Per time bin per Intel(R) Xeon(R) CPU E5-2660 v3 @ 2.60 GHz.
[2] Run in hybrid MPI/OMP mode in 50 nodes of 20 threads each.

This high amount of computational resources could be strongly reduced with the development and application of suitable variance reduction techniques. The success of such techniques could clear the path for further industry-like application with reduced calculation times.

Finally, regarding potential bottlenecks, no serious demand of RAM was observed as far as there is no need for a large amount of materials (usually required to deal with burnup calculations). It should be regarded here that this could not be the case for potential scenarios where the initial configuration requires high number of materials, such as previously burned cases.

6. Main results discussion and further work

From the in-depth analysis of the results presented in Section 5 it should be regarded that:

a. For the CZP and HZP preliminary calculations, a general good agreement was found for TR, isothermal coefficient and excess reactivities. Despite the encountered deviations with the reported values, the level of agreement is found to be as accurate as the specification uncertainties. In addition, those differences are not expected to affect the further transient calculations, as far as no initial position of CR are provided.
b. The HFP transient experiments T-84 and T-85 were calculated with the coupled *Serpent-SCF* novel tool showing very good global results. The capability to develop coupled transient calculation is assessed, thus providing a first step towards the validation of the proposed approach.
c. For both T-84 and T-85 cases, slight differences in the introduced reactivity were observed, indicating that the TR movement modeling as a constant speed could be improved. In addition, the impact of the lack of specification of other modeling parameters that could also affect the transient evolutions (such as the gap conductance) should be considered in further works.
d. The capability to obtain highly-detailed results using this approach was proved, which paves the way to further safety-oriented calculations.
e. A raw estimation of relative CPU requirement is provided, which allows the estimation of resources for more complex problems.

It should be regarded that although the global coupled transient consistency of the approach is validated with experimental results, the level of detail of the reported data (McCardell et al., 1967; Olson, 2015) does not allow to properly check the evolution of *high-fidelity* oriented results (such as pin-by-pin axial dependencies). Unfortunately there is no open literature available providing these highly detailed data, but still further steps are foreseen for the workpath here presented, namely:

i. Develop code to code comparisons with similar tools for the same cases presented here.
ii. Include additional cases where the time scope is increased. The suitable cases available in McCardell et al. (1967) are those for Hot-Standby. Unfortunately, the increase of power for such cases represents several orders of magnitude, which will imply an issue from the statistical convergence point of view.
iii. In-depth analysis and aplication of variance reduction techniques implementations in order to encourage industry-like applications.

7. Conclusions

To tackle the increasing interest on the development of highly accurate methodologies in reactor physics, the McSAFE project is

aimed to develop a wide-range of coupled tools. These tools are designed to provide capabilities for *high-fidelity* multiphysics calculations for steady-state, burnup and transient cases for square and hexagonal geometries.

In this framework, a *Serpent-SCF* coupling scheme developed in terms of a new versatile internal coupling approach is in this work considered. Previous works presented the verification of the consistency for real case geometries, where a proper validation with experimental data was still missing.

A first step towards validation was developed here for this novel approach through a comparison with experimental data. For such purpose, selected experiments from the SPERT-IIIE reactor were calculated with this *high-fidelity* approach. A graded approach was applied, assessing the models and tools capabilies by comparison with experimental reported values ranging from uncoupled cases to coupled transient ones.

A good agreement with experimental data was observed both for cold and hot steady states and for the selected full-power transient ones. These comparisons provide thus a first validation of the approach in terms of global parameters for a geometrical configuration and operational conditions similar to a standard PWR ones. The consistency of this novel approach is then assessed for the final proposed goals, not only from the geometrical point of view, but also from the operational conditions and expected evolution under RIA-scenarios.

Finally, in order to present inherent benefits of this approach, pin-by-pin results were also presented and analyzed for these RIA scenarios from the SPERT-IIIE reactor. As a result, the capability to produce *high-fidelity* results in realistic geometries is assessed. For completness, a raw estimation of resources required for such cases was also included.

The good behaviour encountered in the cases analyzed paves the way to further detailed transient calculations and encourages to continue the path to finally tackle industry-like *high-fidelity* applications.

CRediT authorship contribution statement

Diego Ferraro: Writing - original draft, Writing - review & editing, Resources, Formal analysis, Validation, Software, Methodology, Conceptualization, Visualization. **Manuel García:** Writing - review & editing, Resources, Software, Methodology. **Ville Valtavirta:** Writing - review & editing, Resources, Software. **Uwe Imke:** Writing - review & editing, Resources, Software. **Riku Tuominen:** Writing - review & editing, Resources, Software. **Jaakko Leppänen:** Writing - review & editing, Supervision, Resources, Software. **Victor Sanchez-Espinoza:** Writing - review & editing, Funding acquisition, Project administration, Supervision.

Declaration of Competing Interest

The authors declare that they have no known competing financial interests or personal relationships that could have appeared to influence the work reported in this paper.

Acknowledgments

This work was done within the McSAFE project which is receiving funding from the Euratom research and training programme 2014-2018 under grant agreement No 755097. This work was performed on the computational resource ForHLR II, funded by the Ministry of Science, Research and the Arts Baden-Württemberg and DFG (“Deutsche Forschungsgemeinschaft”).

References

Cao, L., Gerlach, A., Xu, Y., Downar, T., Lee, J.C., 2015. Neutronics modeling of the SPERT III E-Core critical experiments with MPACT and KENO. Ann. Nucl. Energy 80. https://doi.org/10.1016/j.anucene.2015.02.013.

CASL – a DOE Energy Innovation Hub for Modeling and Simulation of Nuclear Reactors, The Consortium for Advanced Simulation of Light Water Reactors, URL: https://www.casl.gov/, Online; (Accessed 17.08.2018 (2010-2018)). .

Chadwick, M. et al., 2011. ENDF/B-VII.1 Nuclear data for science and technology: cross sections, covariances, fission product yields and decay data. Nuclear Data Sheets 112 (12), 2887–2996. https://doi.org/10.1016/j.nds.2011.11.002. Special Issue on ENDF/B-VII.1 Library.

Ferraro, D. et al., 2019. Serpent and TRIPOLI-4® transient calculations comparisons for several reactivity insertion scenarios in a 3D PWR minicore benchmark. In: International Conference on Mathematics and Computational Methods applied to Nuclear Science and Engineering (M&C 2019).

Ferraro, D. et al., 2020. Serpent/SUBCHANFLOW pin-by-pin coupled transient calculations for a PWR minicore. Annals of Nuclear Energy 137, 107090. https://doi.org/10.1016/j.anucene.2019.107090.

Ferraro, D., et al., 2018. Foreseen capabilities, bottlenecks identification and potential limitations of Serpent MC transport code in large-scale full 3-D burnup calculations. In: Proceedings of the 26th International Conference on Nuclear Engineering – ICONE26, London, England..

García, M. et al., 2020. Serpent2-SUBCHANFLOW pin-by-pin modelling capabilities for VVER geometries. Ann. Nucl. Energy 135, 106955. https://doi.org/10.1016/j.anucene.2019.106955.

Imke, U. et al., 2012. Validation of the Subchannel Code SUBCHANFLOW Using the NUPEC PWR Tests (PSBT). Sci. Technol. Nucl. Install. 12. https://doi.org/10.1155/2012/465059. URL: http://downloads.hindawi.com/journals/stni/2012/465059.pdf.

Imke, U., 2018. User manual for SUBCHANFLOW 3.6.1, Tech. rep., Karlsruhe Institute for Technology – Institute for Neutron Physics and Reactor Technology. .

Leppänen, J., 2013. Modeling of nonuniform density distributions in the serpent 2 Monte Carlo code. Nucl. Sci. Eng. 174 (3), 318–325. https://doi.org/10.13182/NSE12-54.

Leppänen, J. et al., 2013. The Serpent Monte Carlo code: Status, development and applications in 2013. Ann. Nucl. Energy 82, 142–150. https://doi.org/10.1016/j.anucene.2014.08.024.

Leppänen, J., et al., 2013. Development of a dynamic simulation mode in the Serpent 2 Monte Carlo code. In: M&C 2013. .

Levinsky, A., Valtavirta, V., Adams, F., Anghel, V., 2019. Modeling of the SPERT transients using Serpent 2 with time-dependent capabilities. Ann. Nucl. Energy 125, 80–98. https://doi.org/10.1016/j.anucene.2018.09.038.

Luigi Mercatali et al., 2017. McSafe projects Highlights – Available in NUGENIA project portfolio, available at URL: https://www.ne.ncsu.edu/event/workshop-international-multi-physics-validation/, Presentation at International MultiPhysics Validation Workshop North Carolina State University (June 2017)..

McCardell, R.K., Herborn, D.I., Houghtaling, J.E., 1967. Reactivity Accident Test Results and Analyses for the SPERT III E-Core, Technical Report IDO-17281 Phillips Petroleum Co, US Atomic Energy Commission (AEC) URL: https://www.osti.gov/biblio/4792676..

Olson, A.P., 2013. Neutronics Calculations for SPERT-III, E-core, Nuclear Engineering Division, Argonne National Laboratory (ANL/GTRI/TM-13/10). https://doi.org/10.2172/1087815. .

Olson, Arne P., 2015. SPERT III E CORE: FACILITY SPECIFICATION, IAEA Technical Report Series No. 480, available at URL: https://www.iaea.org/publications/10578. .

RJ McConn, 2011. Compendium of Material Composition Data for Radiation Transport Modeling, PNNL-15870 Rev. 1. .

Santamarina, A., et al., 2009. The JEFF-3.1.1 Nuclear Data Library, Tech. Rep. JEFF Report 22 – ISBN 978-92-64-99074-6, NUCLEAR ENERGY AGENCY (NEA) – Organisation for Economic Co-operation and Development, available at URL: http://www.oecd-nea.org/dbdata/nds_jefreports/jefreport-22/nea6807-jeff22.pdf..

Serpent developer team, 2018. Serpent Wiki on-line user Manual for Serpent 2, URL: http://serpent.vtt.fi/mediawiki/index.php/Main_Page, Online; (Accesed 25.09.2019).

Valtavirta, V., 2017. Development and applications of multiphysics capabilities in a continuous energy Monte Carlo neutron transport code (Ph.D. thesis). Aalto University, School of Science, Department of Applied Physics, Finland, iSBN 978-952-60-7377-4 – Available at URL: http://montecarlo.vtt.fi/download/S150.pdf. .

Valtavirta, V., et al., 2016. Delayed Neutron Emission Model for Time Dependent Simulations with the Serpent 2 Monte Carlo Code – First Results. In: Physor 2016..

Viitanen, T., Leppänen, J., 2014. Target motion sampling temperature treatment technique with elevated basis cross-section temperatures. Nucl. Sci. Eng. 177 (1), 77–89. https://doi.org/10.13182/NSE13-37.

Zoia, A., Brun, E., 2016. Reactor physics analysis of the SPERT III E-core with Tripoli-4. Ann. Nucl. Energy 90, 71–82. https://doi.org/10.1016/j.anucene.2015.11.032.